$Fe^{II}(TPA) + H_2O_2$

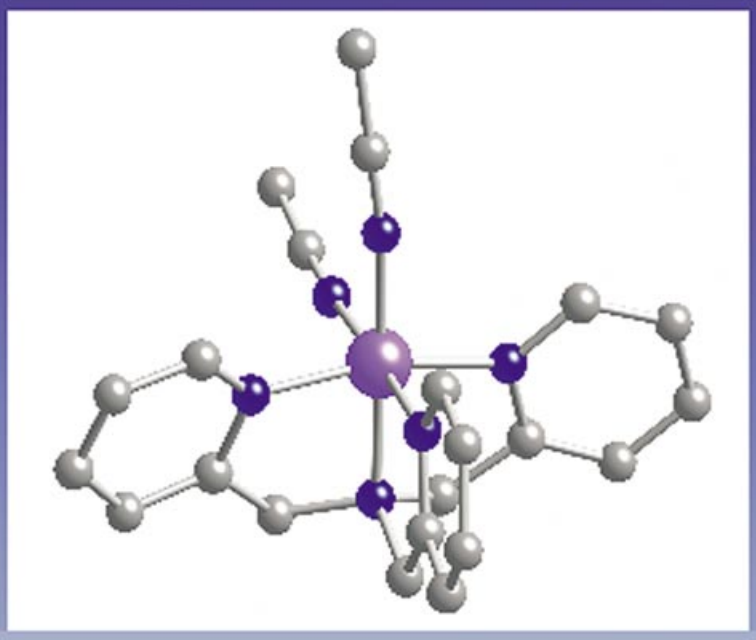

Distinct Intermediates in CH_3CN and Acetone, but Similar Oxidation Catalysis

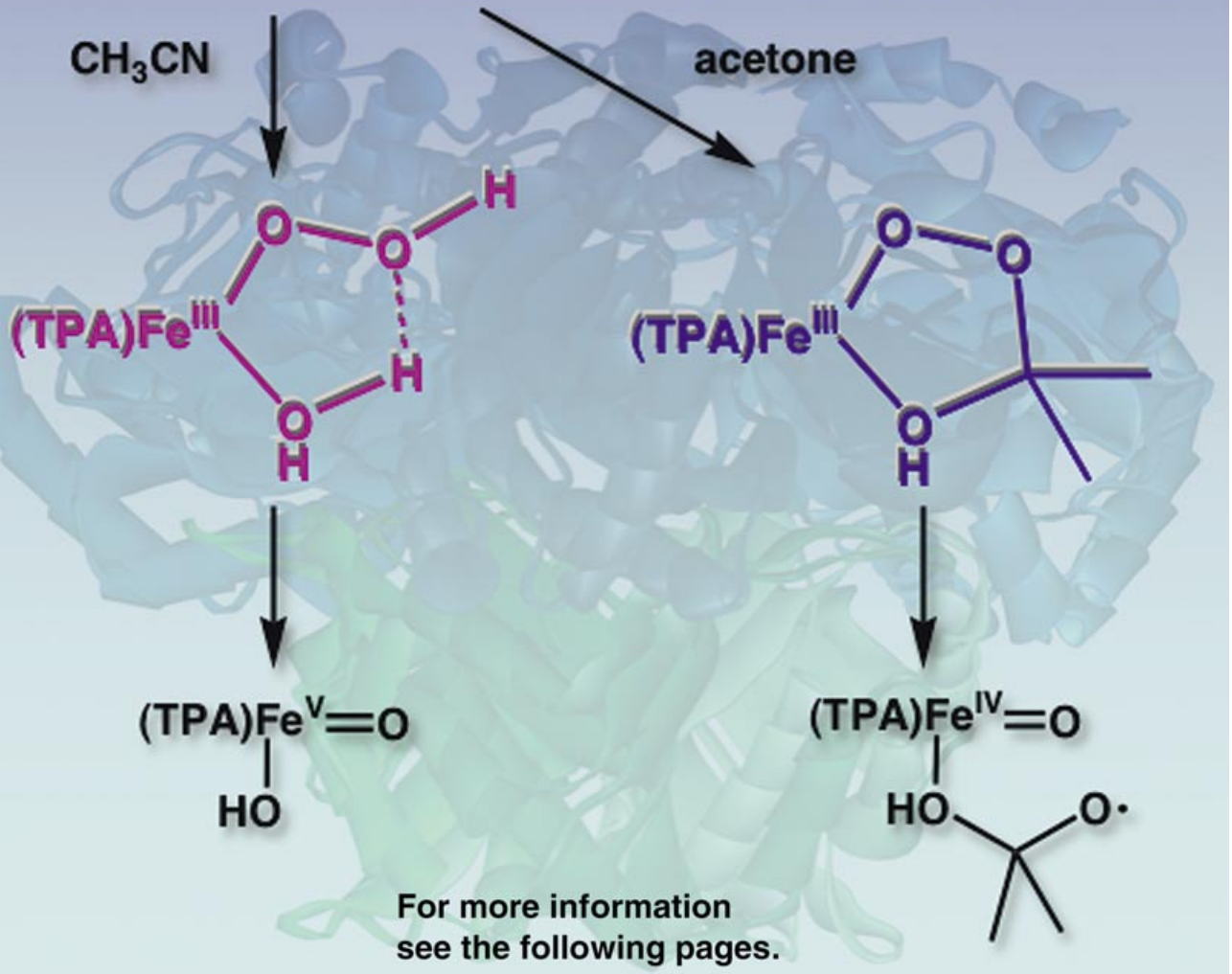

DOI: 10.1002/chem.200400480 *Chem. Eur. J.* **2004**, *10*, 4944 – 4953

The Reaction of $[Fe^{II}(tpa)]$ with H_2O_2 in Acetonitrile and Acetone—Distinct Intermediates and Yet Similar Catalysis

Antoni Mairata i Payeras, Raymond Y. N. Ho, Megumi Fujita, and Lawrence Que, Jr.*[a]

Abstract: The reaction of $[Fe^{II}(tpa)(OTf)_2]$ (tpa = tris(2-pyridylmethyl)-amine) and its related 5-Me_3-tpa complex with hydrogen peroxide affords spectroscopically distinct iron(III)–peroxo intermediates in CH_3CN and acetone. The reaction in acetonitrile at −40 °C results in the formation of the previously reported Fe^{III}–OOH intermediate, the end-on hydroperoxo coordination mode of which is established in this paper by detailed resonance Raman isotope-labeling experiments. On the other hand, the reaction in acetone below −40 °C leads to the observation of a different peroxo intermediate identified by resonance Raman spectroscopy to be an Fe^{III}–OOC$(CH_3)_2$OH species; this represents the first example of an intermediate derived from the adduct of H_2O_2 and acetone. The peroxoacetone intermediate decays more rapidly than the corresponding Fe^{III}–OOH species and converts to an Fe^{IV}=O species by O–O bond homolysis. This decay process is analogous to that observed for $[Fe^{III}(tpa)(OOtBu)]^{2+}$ and in fact exhibits a comparable enthalpy of activation of 54(3) kJ mol^{-1}. Thus, with respect to their physical properties at low temperature, the peroxoacetone intermediate resembles $[Fe^{III}(tpa)(OOtBu)]^{2+}$ more than the corresponding Fe^{III}–OOH species. At room temperature, however, the behavior of the Fe(tpa)/H_2O_2 combination in acetone in catalytic hydrocarbon oxidations differs significantly from that of the Fe(tpa)/*t*BuOOH combination and more closely matches that of the Fe(tpa)/H_2O_2 combination in CH_3CN. Like the latter, the Fe(tpa)/H_2O_2 combination in acetone catalyzes the hydroxylation of *cis*-1,2-dimethylcyclohexane to its tertiary alcohol with high stereoselectivity and carries out the epoxidation and *cis*-dihydroxylation of olefins. These results demonstrate the subtle complexity of the Fe(tpa)/H_2O_2 reaction surface.

Keywords: homogeneous catalysis · hydrogen peroxide · iron · O–O bond homolysis · oxidation · oxo ligands

Introduction

Iron–peroxo species are frequently invoked as intermediates in the catalytic cycles of mononuclear nonheme iron enzymes involved in dioxygen metabolism.[1–3] Direct experimental evidence is now available for such intermediates in the chemistry of superoxide reductase,[4,5] naphthalene dioxygenase,[6] and lipoxygenase,[7] as well as for that of the antitumor drug bleomycin.[8] In mechanisms of oxygen-activating iron enzymes, peroxo intermediates serve as precursors to higher valent iron–oxo species that effect the oxidative transformation of substrate.[3] To gain insight into this fascinating chemistry, we have had a long standing effort in the design and synthesis of functional models for such systems. We have recently identified a particularly intriguing family of iron complexes based on $[Fe^{II}(tpa)(CH_3CN)_2]^{2+}$ (**1**, tpa = tris(2-pyridylmethyl)amine) that act as catalysts for the H_2O_2-mediated hydroxylation of alkanes to alcohols and olefins to epoxides and *cis*-diols with high stereoselectivity.[9] The observed *cis*-dihydroxylation of olefins in fact represents the first such example catalyzed by an iron complex. More recently, Feringa and co-workers reported catalytic oxidation studies with a related complex, $[Fe^{II}$(N3Py-

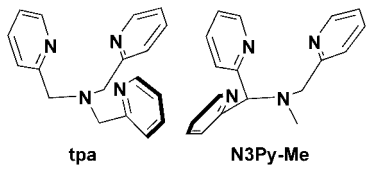

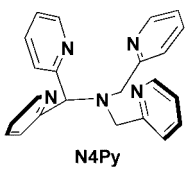

[a] Dr. A. Mairata i Payeras, Dr. R. Y. N. Ho, Dr. M. Fujita, Prof. Dr. L. Que, Jr.
Department of Chemistry
and Center for Metals in Biocatalysis
University of Minnesota, 207 Pleasant St. SE
Minneapolis, Minnesota 55455 (USA)
Fax: (+1) 612-624-7029
E-mail: que@chem.umn.edu

 DOI: 10.1002/chem.200400480

Me)$(CH_3CN)_2]^{2+}$ (N3Py-Me = *N*-methyl-*N*-2-pyridylmethyl-bis(2-pyridyl)methylamine), which showed catalytic behavior in CH_3CN similar to that reported for Fe(tpa) complex in the same solvent.[10] However the oxidation chemistry in acetone solvent was different; in particular, the dihydroxylation of cyclooctene afforded the *trans*-diol instead.

These results led us to compare the Fe(tpa)/H_2O_2 combination in the two solvents. Previously, we had trapped a transient purple intermediate at −40 °C in CH_3CN and identified it as $[Fe^{III}(tpa)(OOH)]^{2+}$.[11,12] In this paper, we provide a more detailed Raman characterization of the purple intermediate in CH_3CN that establishes it unequivocally as $[Fe^{III}(tpa)(\eta^1\text{-}OOH)]^{2+}$. Based on ^{18}O-labeling experiments, this intermediate was proposed to convert to $[Fe^{V}{=}O\text{-}(tpa)(OH)]^{2+}$, which is responsible for highly stereoselective alkane hydroxylation and olefin epoxidation and *cis*-dihydroxylation.[13,14] In acetone, a different peroxo intermediate is formed; this undergoes O–O bond homolysis to form an observed iron(IV)–oxo species at −50 °C. Yet the oxidation catalysis observed at room temperature affords products remarkably similar to those reported for the same catalyst in CH_3CN. These apparently contradictory observations are rationalized within a common mechanistic framework.

Results and Discussion

Detailed Raman characterization of $[Fe^{III}(tpa)(OOH)]^{2+}$ in CH_3CN: Previously, we reported that the addition of excess hydrogen peroxide to $[Fe^{II}(tpa)]^{2+}$ or $[Fe^{III}_2(\mu\text{-}O)\text{-}(tpa)_2(OH_2)_2]^{4+}$ in CH_3CN at −40 °C gave rise to a low-spin $[Fe^{III}(tpa)(OOH)]^{2+}$ intermediate that has been characterized by its visible absorption and EPR spectroscopy and electrospray mass spectrometry.[11,14] The intermediate exhibits a visible absorption maximum at 538 nm ($\varepsilon \sim 1000\ M^{-1}cm^{-1}$) and an EPR spectrum with *g* values of 2.19, 2.15 and 1.97 (Figure 1). This species decayed upon standing or upon warming to room temperature to a species with NMR features at $\delta = 2.2$, 6.2, 19, and ~32 ppm (br), suggesting that the decay product is mainly $[Fe^{III}_2(\mu\text{-}O)\text{-}(tpa)_2(OH_2)_2]^{4+}$. Unlike the closely related low-spin $[Fe^{III}(N4Py)(OOH)]^{2+}$ (N4P*y* = *N*,*N*-bis(2-pyridylmethyl)-bis(2-pyridyl)methylamine), this hydroperoxo intermediate has proved more difficult to study by resonance Raman spectroscopy due to 1) bleaching of the chromophore upon freezing and 2) photodecomposition under the laser beam.

We thus explored different conditions to obtain better quality Raman spectra. We first explored the use of mixed-solvent systems with freezing points below −45 °C (the freezing point of CH_3CN) to increase the stability of the intermediate. We obtained a resonance Raman spectrum of the intermediate in CD_3CN/THF (4:1),[12] showing vibrational features at 627 and 789 cm^{-1}

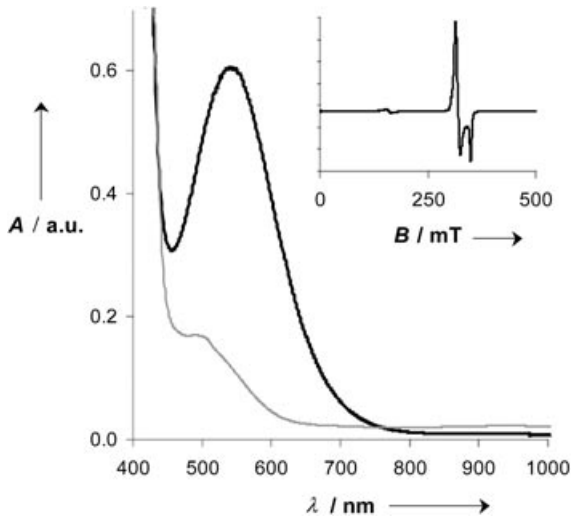

Figure 1. Visible spectra of the $[Fe^{III}(tpa)(OOH)]^{2+}$ chromophore obtained by the addition of 10 equivalents of H_2O_2 to a 1 mM solution of $[Fe^{II}(tpa)(OTf)_2]$ in acetonitrile at −45 °C (black line) and its decay product (gray line). Inset: EPR spectrum of $[Fe^{III}(tpa)(OOH)]^{2+}$ in acetonitrile at 2 K.

(Table 1, entry 1) similar to those observed for $[Fe^{III}(N4Py)(OOH)]^{2+}$ (Table 1, entries 9 and 10).[15] We eventually obtained good spectra in liquid CH_3CN in a spinning cell maintained at −44 °C by using low laser power (Table 1, entry 2). Following a report by Talsi and co-workers that $[Fe^{III}(tpa)(OOH)]^{2+}$ could be observed at −60 °C in liquid CH_3CN/CH_2Cl_2 (1:1),[16] we also found that the $[Fe^{III}\text{-}(tpa)(OOH)]^{2+}$ intermediate in 1:1 CD_3CN/CD_2Cl_2 could be frozen without loss of chromophore and gave rise to good quality Raman spectra (Table 1, entry 3; Figure 2A left panel). The vibrations observed for $[Fe^{III}(tpa)(OOH)]^{2+}$ under these various conditions do not differ significantly (Table 1). At this point it is unclear what makes $[Fe^{III}\text{-}(tpa)(OOH)]^{2+}$ in pure CH_3CN bleach upon freezing.

To unequivocally establish the binding mode of the hydroperoxo ligand in $[Fe^{III}(tpa)(OOH)]^{2+}$, resonance Raman experiments with $H_2{}^{18}O_2$ were essential. However, the high fraction of water in the commercially available 2% $H_2{}^{18}O_2$ solution resulted in a significantly lower yield of the desired intermediate, presumably due to competitive formation of the corresponding (μ-oxo)diiron(III) complex. This problem was overcome by pre-drying the H_2O_2 solution in an appropriate organic solvent with $MgSO_4$. The combination of a lower freezing solvent and the dried H_2O_2 solution afforded

Table 1. Resonance Raman data for the peroxo species formed upon reaction of H_2O_2 or *t*BuOOH with $[Fe(L)]^{2+}$ complexes in frozen solution, except where noted.

Entry	Ligand/peroxide	Solvent	ν(Fe–OOR) [cm^{-1}]	ν(O–O) [cm^{-1}]
1[12]	tpa/H_2O_2	CD_3CN/THF (4:1, liquid)	626	789
2	tpa/H_2O_2	CD_3CN (liquid)	624	806
3	tpa/H_2O_2	CD_3CN/CD_2Cl_2 (1:1)	624	803
4	5-Me_3-tpa/H_2O_2	CD_3CN	635	800
5	tpa/H_2O_2	$(CH_3)_2CO$	692	–
6	tpa/H_2O_2	$(CD_3)_2CO$	681	793/811
7[17]	tpa/*t*BuOOH	CH_3CN	696	796
8[17]	tpa/[D_9]*t*BuOOH	CH_3CN	668/700	803
9[12]	N4Py/H_2O_2	$(CD_3)_2CO$	632	790
10[15]	N4Py/H_2O_2	CH_3OH	632	790

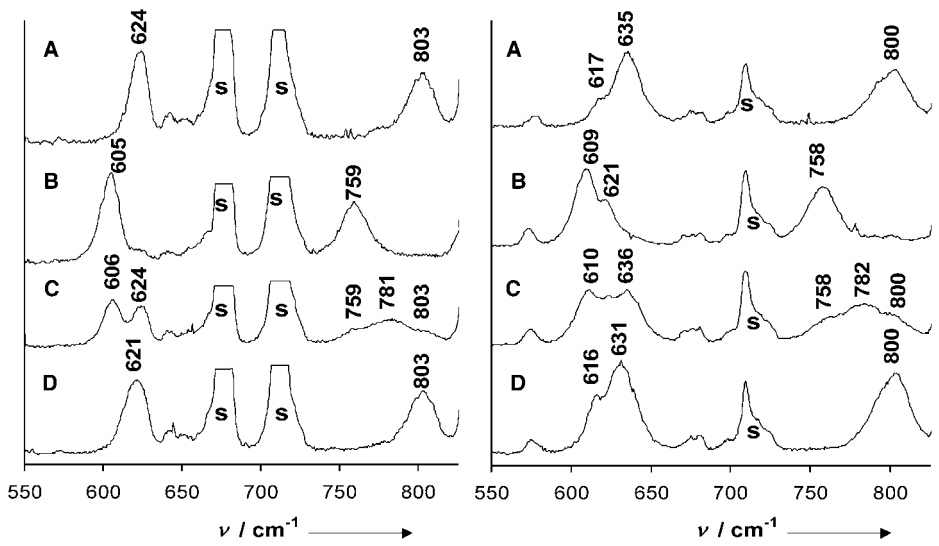

Figure 2. Resonance Raman spectra (λ_{ex} 568.2 nm) of $[Fe^{III}(tpa)(OOH)]^{2+}$ in 1:1 CD_3CN/CD_2Cl_2 (left panel) and $[Fe^{III}(5\text{-}Me_3\text{-}tpa)(OOH)]^{2+}$ in CD_3CN (right panel). Individual spectra in each panel represent experiments with $H_2{}^{16}O_2$ (A), $H_2{}^{18}O_2$ (B), 50% ^{18}O-labeled H_2O_2 (C), and $D_2{}^{16}O_2$ (D).

the spectra shown in Figure 2 left panel. Thus with $H_2{}^{18}O_2$, the features observed at 803 and 624 cm^{-1} in the $H_2{}^{16}O_2$ spectrum (Figure 2A left panel) shift to 759 and 605 cm^{-1}, respectively (Figure 2B left panel). The downshift of 44 cm^{-1} for the 803 cm^{-1} peak is fully consistent with its assignment as ν(O–O) ($\Delta\nu_{calcd} = -46$ cm^{-1}). Similarly, the downshift of 19 cm^{-1} for the 624 cm^{-1} peak approaches the value of 22 cm^{-1} predicted by Hooke's law for an Fe–OOH vibration. With 50% ^{18}O-labeled H_2O_2 (Figure 2C left panel), the ν(O–O) feature splits into three peaks at 759, 781, and 803 cm^{-1} with an intensity ratio of 1:2:1, while the ν(Fe–OOH) feature becomes two equally intense peaks at 606 and 624 cm^{-1}. Finally, the experiment with D_2O_2 shows no effect on ν(O–O) and a downshift of 3 cm^{-1} for ν(Fe–OOH) (Figure 2D left panel). Taken together, the Raman data support the notion that the $[Fe^{III}(tpa)(OOH)]^{2+}$ intermediate has an end-on bound hydroperoxide ligand, as found earlier for $[Fe^{III}(N4Py)(OOH)]^{2+}$.[12,15]

Subsequent to this effort, we learned that the use of $[Fe^{II}(5\text{-}Me_3\text{-}tpa)(OTf)_2]$ (5-Me_3-tpa = tris(5-methylpyridyl-2-methyl)amine) in place of $[Fe^{II}(tpa)(OTf)_2]$ as precursor led to a more stable Fe^{III}–OOH intermediate, presumably due to the introduction of the electron-donating 5-methyl substituents. Thus this Fe^{III}–OOH intermediate can be studied in frozen CH_3CN without loss of chromophore (Table 1, entry 4). Parallel isotope-labeling experiments on $[Fe^{III}(5\text{-}Me_3\text{-}tpa)(OOH)]^{2+}$ confirmed results reported above for $[Fe^{III}(tpa)(OOH)]^{2+}$ in CD_3CN/CD_2Cl_2 (Figure 2 right panel, Table 1).

Reaction of $[Fe^{II}(tpa)(OTf)_2]$ and H_2O_2 in acetone: Our exploration of suitable low-temperature solvents also led us to study the formation of the $[Fe^{III}(tpa)(OOH)]^{2+}$ intermediate in acetone, and different results were obtained. The reaction of $[Fe^{II}(tpa)(OTf)_2]$ and a small excess of H_2O_2 in acetone at −40 °C resulted in the formation of an intermediate with a λ_{max} at 523 nm that was less stable than that in acetonitrile; the species decayed completely after approximately two minutes at this temperature. When the reaction was performed at −90 °C, the intermediate persisted for at least three hours. A minimum of 1.5 equivalents of H_2O_2 to the iron(II) precursor was required to reach maximum absorbance at 523 nm (Figure 3), consistent with its expected formulation as an iron(III)–peroxo complex (0.5 equivalents for the initial oxidation of iron(II) to iron(III)) and 1 equivalent to form the peroxo complex). Its EPR spectrum revealed an $S = 1/2$ center with g values at 2.22, 2.16, and 1.98, similar to those of $[Fe^{III}(tpa)(OOH)]^{2+}$ or $[Fe^{III}(tpa)(OO\mathit{t}Bu)]^{2+}$ in CH_3CN (Figure 3 inset, Table 2).

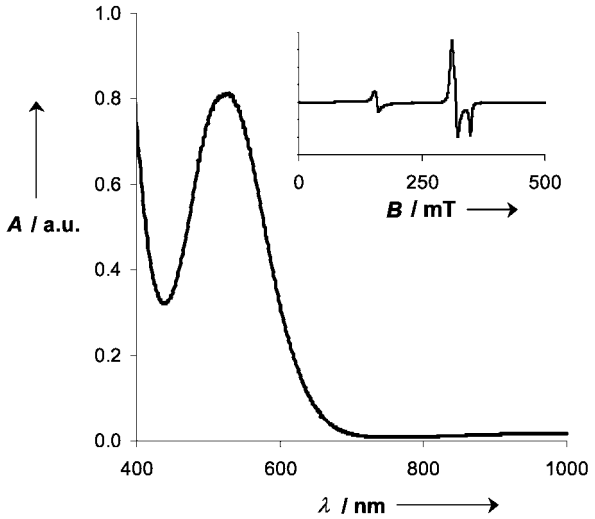

Figure 3. Visible spectrum of the species formed upon addition of 1.5 equiv H_2O_2 to a solution of $[Fe^{II}(tpa)(OTf)_2]$ in acetone at −90 °C. Inset: EPR spectrum at 2 K taken of the solution after maximization of the chromophore at 523 nm.

Table 2. Spectroscopic data on low-spin [Fe(tpa)OOR] intermediates; R is −H, $-C(CH_3)_2OH$, or $-C(CH_3)_3$.

Entry	Oxidant	Solvent	λ_{max} (ε)	EPR g values
1[11]	H_2O_2	CH_3CN	538 (1050)	2.19, 2.15, 1.97
2	H_2O_2	CH_3CN/THF (1:1)	540	2.20, 2.14, 198
3	H_2O_2	CH_3CN/CD_2Cl_2	528	2.20, 2.16, 1.97, 2.18, 2.12, 1.97
4[16]	H_2O_2	$CH_3CN/CH_2Cl_2/CH_3OH$	–	2.196, 2.126, 1.972
5	H_2O_2	$(CH_3)_2CO$	523 (1200)	2.22, 2.16, 1.98
6	H_2O_2	$(CH_3)_2CO$/PyO	518 (700)	2.22, 2.16, 1.97
7[18]	*t*BuOOH	CH_3CN	600 (2200)	2.19, 2.14, 1.98
8	*t*BuOOH	dry CH_3CN	590 (2200)	2.15, 2.11, 1.96

Integration of the low-spin EPR signal against a $Cu(SO_4)_2$ standard gave an estimated extinction coefficient of 1200 $M^{-1}cm^{-1}$ for the chromophore with λ_{max} at 523 nm. Based on the systematic EPR studies of Talsi on iron–peroxo complexes,[16] the lower field position of the g_{max} value suggests that the sixth ligand in this complex is likely to be an oxygen atom.

The resonance Raman spectrum of the 523 nm intermediate in acetone showed features distinct from those observed in CH_3CN. Only one resonance enhanced peak was clearly observed in the ν(Fe–O) region at 692 cm^{-1}, while the ν(O–O) region was obscured by solvent vibrations. However, the use of [D_6]acetone resulted in the downshift of the 692 cm^{-1} peak to 681 cm^{-1} and the unmasking of features at 793 and 811 cm^{-1} (Figure 4). This pattern of frequencies is more typical of a low-spin Fe^{III}–OOR complex (Table 1, entry 7), and not of a low-spin Fe^{III}–OOH complex (Table 1, entries 1–4, 9 and 10). Moreover, the observation that the use of [D_6]acetone causes the 692 cm^{-1} peak to downshift suggests that acetone is incorporated into the intermediate species. In support, Raman studies of Fe^{III}–OO*t*Bu complexes showed that deuteration of the *tert*-butyl group resulted in the downshift and splitting of a feature at 696 cm^{-1} (Table 1, entry 8).[17] Normal coordinate analysis of the [Fe^{III}-(tpa)(OO*t*Bu)]$^{2+}$ intermediate revealed that this vibration consists of a mixture of Fe–O and C–O stretching modes and alkoxyl deformations.[19] Thus, the intermediate observed in acetone is formulated as an Fe^{III}(tpa) complex with a bound $-OOC(CH_3)_2(OH)$ group derived from peroxide addition to acetone. A similar species was suggested to form by Feringa and co-workers in studies of catalytic hydrocarbon oxidation with the Fe(N3Py-Me) complex, but no direct experimental evidence was provided.[10]

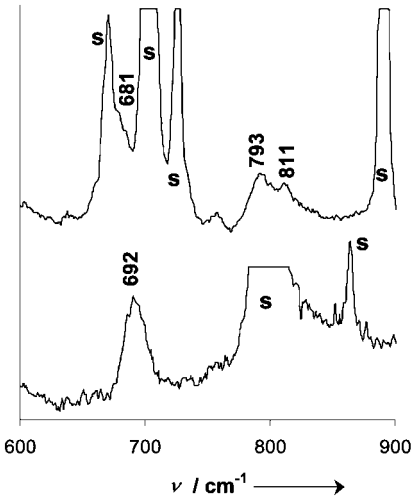

Figure 4. Resonance Raman spectra of the Fe(tpa)/H_2O_2 chromophore in acetone (bottom) and [D_6]acetone (top). λ_{ex} 514.5 nm.

The observation of a bound peroxoacetone moiety raises the question of how such a species is formed. It is known from the literature[20] that hydrogen peroxide exists in acetone in equilibrium with the 2-hydroxy-2-hydroperoxypropane (HHPP) adduct [Eq. (1)]:

$$CH_3COCH_3 + H_2O_2 \rightleftharpoons (CH_3)_2C(OH)(OOH) \quad (1)$$

At 0 °C, ~75 % of the hydrogen peroxide in acetone is present as HHPP as monitored by NMR spectroscopy. Given the measured equilibrium constant, we calculate that, under our reaction conditions (−50 to −90 °C), more than 98 % of the peroxide is present as HHPP, which reacts with the iron(II) precursor to form the intermediate directly.

In contrast, the reaction of H_2O_2 and [Fe^{II}(N4Py)(CH_3CN)]$^{2+}$ in acetone did not give rise to the HHPP intermediate, but instead afforded [Fe^{III}(N4Py)(OOH)]$^{2+}$.[15,21] The resonance Raman spectra of the intermediate in CH_3OH and acetone are essentially identical (Table 1) and very similar to that associated with [Fe^{III}(tpa)(OOH)]$^{2+}$. Since pentadentate N4Py and tetradentate tpa only differ in having an additional pyridine ligand for the former, this observation suggests that the formation of the HHPP complex may be enhanced by the presence of a coordination site on the Fe(tpa) center for the 2-hydroxy group of HHPP to form a five-membered chelate ring.

While the Fe^{III}–$OOC(CH_3)_2OH$ intermediate was stable at −90 °C, warming to room temperature resulted in its decay to a species that has a multifeatured UV-visible spectrum characteristic of [Fe_2(μ-O)(O_2CCH_3)(tpa)$_2$]$^{3+}$ (Figure 5, gray line).[22] Based on its well-established extinction coefficients, the (μ-oxo)diiron(III) complex appeared to be quantitatively formed from the iron(II) complex. Since no carboxylate was present at the start of the reaction, it must be produced in the course of peroxo decay. Electrospray mass spectrometric analysis confirmed the formation of [Fe^{III}_2O(O_2CCH_3)(tpa)$_2$]$^{3+}$. When the reaction was carried out in [D_6]acetone, the expected increase of three units in

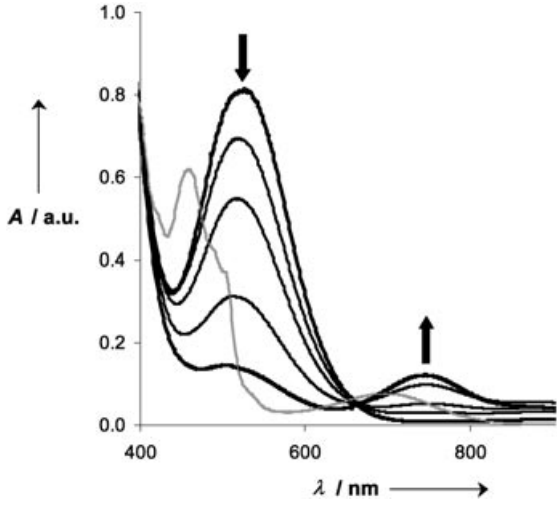

Figure 5. UV-visible spectral changes observed in the conversion of [Fe^{III}(tpa)($OOC(CH_3)_2OH$)]$^{2+}$ to [Fe^{IV}(O)tpa]$^{2+}$ in acetone from −90 to −50 °C (black lines) and its room temperature decay product [Fe^{III}_2(μ-O)(O_2CCH_3)(tpa)$_2$]$^{3+}$ (gray line).

the mass of the molecular ion of the product was observed (Figure 6), demonstrating that the acetone solvent was indeed the source of the acetate bridge. Thus the peroxo intermediate must decay by a pathway that results in C–C bond cleavage of an acetone molecule, presumably the one incorporated into the HHPP intermediate.

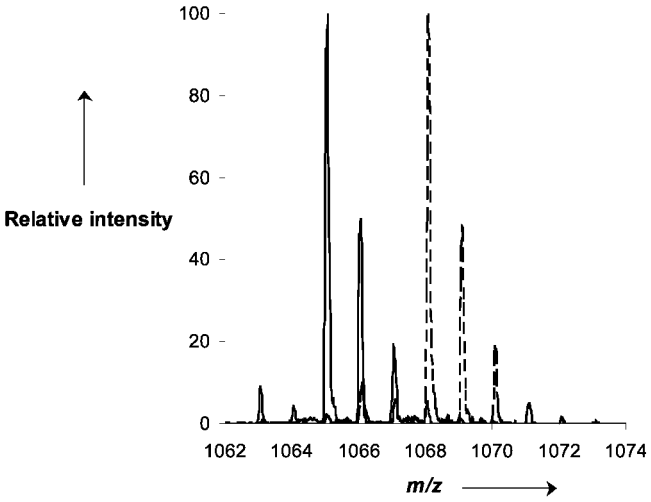

Figure 6. Electrospray mass spectra of the decay product in the reaction of $[Fe^{II}(tpa)(OTf)_2]$ with H_2O_2 in acetone (solid line) and acetone[D_6] (dashed line). The molecular ion corresponds to the $\{[Fe_2(O)(O_2CCH_3)(tpa)_2](OTf)_2\}^+$ ion.

Warming the acetone solution of the Fe^{III}–$OOC(CH_3)_2OH$ intermediate from −90 to −50 °C showed the formation of a new species with λ_{max} at 742 nm with an apparent isosbestic point at abbout 650 nm (Figure 5). This new species can be assigned to an $[Fe^{IV}(O)(tpa)]^{2+}$ species on the basis of its characteristic near IR absorption band. $[Fe^{IV}(O)(tpa)]^{2+}$ was previously observed to form from the stoichiometric reaction of $[Fe^{II}(tpa)(CH_3CN)_2]^{2+}$ and peracetic acid in CH_3CN ($\lambda_{max}=724$ nm);[23] in acetone the corresponding reaction afforded an intermediate with a λ_{max} at 738 nm. The red shift observed is likely due to the substitution of CH_3CN as the sixth ligand with acetone. While the 1:1 stoichiometry of the peracid reaction strongly suggests that $[Fe^{IV}(O)(tpa)]^{2+}$ forms by O–O bond heterolysis; its formation from the Fe^{III}–HHPP intermediate must be a result of O–O bond homolysis, as recently reported for the decay of $[Fe^{III}(tpa)(OO\textit{t}Bu)]^{2+}$ in CH_3CN.[24] Like the latter, the conversion of $[Fe^{III}(tpa)(OOC(CH_3)_2OH)]^{2+}$ to $[Fe^{IV}(O)(tpa)]^{2+}$ was significantly accelerated by the addition of pyridine *N*-oxide, when it was added after maximal formation of the HHPP intermediate in acetone at −90 °C (Figure 7). Interestingly, upon the addition of pyridine *N*-oxide, there was an immediate blue shift in the absorption maximum of the HHPP intermediate from 523 to 518 nm followed by its fast decay to $[Fe^{IV}(O)(tpa)]^{2+}$ (Figure 7); this blue shift probably reflects the coordination of pyridine *N*-oxide to the metal center of the HHPP intermediate prior to its decay.

Analysis of the temperature dependence of the observed rates for the decay of $[Fe^{III}(tpa)(OOC(CH_3)_2OH)]^{2+}$ and the formation of $[Fe^{IV}(O)(tpa)]^{2+}$ in acetone afforded activation enthalpies that are identical within experimental error for both processes, $\Delta H^{\neq}=54(3)$ kJ mol^{-1}, and $\Delta S^{\neq}$ values of −35(13) and −42(12) J mol^{-1} K^{-1} at 213 K, respectively (Figure 8). This observation strongly suggests that the same rate-determining step connects these two species. The observed $\Delta H^{\neq}$ value is comparable to that for the decay of $[Fe(tpa)(OO\textit{t}Bu)]^{2+}$ in CH_3CN (52 kJ mol^{-1}).[24]

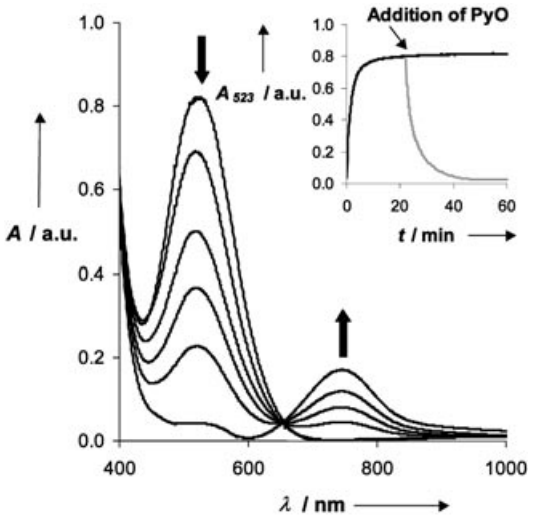

Figure 7. UV-visible spectral changes upon addition of 12 equivalents of pyridine *N*-oxide to $[Fe^{III}(tpa)(OOC(CH_3)_2OH)]^{2+}$ in acetone at −90 °C. Inset: Kinetic trace of the formation of $[Fe^{III}(tpa)(OOC(CH_3)_2OH)]^{2+}$ in acetone at −90 °C by reacting 1 mM $[Fe^{II}(tpa)(OTf)_2]$ with 3 equivalents of H_2O_2 monitored at 523 nm (black lines) and the effect of adding 12 equivalents of pyridine *N*-oxide after maximal formation of the intermediate (gray line).

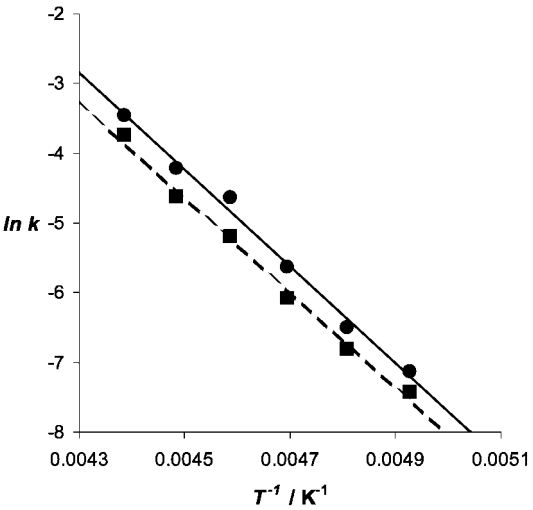

Figure 8. Arrhenius plot for the decay of the $[Fe^{III}(tpa)(OOC(CH_3)_2OH)]^{2+}$ chromophore in acetone (solid line) and the formation of $[Fe^{IV}(O)tpa]^{2+}$ (dashed line).

Taken together, the accumulated information allows us to postulate a mechanism for the reaction of $[Fe^{II}(tpa)(OTf)_2]$ with H_2O_2 in acetone (Scheme 1). Initially, hydrogen perox-

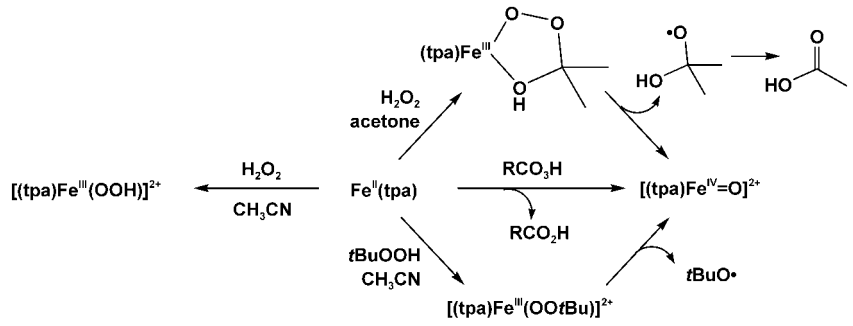

Scheme 1.

ide reacts with acetone to form HHPP, which, after oxidation of Fe^{II} to Fe^{III}, binds to the iron. The complex formed is a metastable $[Fe^{III}(tpa)(\kappa^2\text{-}OOC(CH_3)_2OH)]^{2+}$ species, which then decays to $[Fe^{IV}(O)tpa]^{2+}$ through homolytic cleavage with concomitant C–C bond cleavage to form acetic acid and a methyl radical. Finally, the metastable high-valent species, $[Fe^{IV}(O)tpa]^{2+}$, decays to form $[Fe^{III}_2(\mu\text{-}O)(O_2CCH_3)(tpa)_2]^{3+}$ with incorporation of acetate derived from acetone.

Catalysis at room temperature: The observation of distinct peroxo intermediates documented above at low temperature in CH_3CN and acetone raises the question of what impact these differences may have on the oxidation catalysis by the Fe(tpa)/H_2O_2 combination at room temperature. In particular, the demonstrated formation of a peroxoacetone intermediate at low temperature and its subsequent homolysis to form an $[Fe^{IV}(O)(tpa)]$ species resembles more the chemistry of the Fe(tpa)/*t*BuOOH combination in CH_3CN[24] than that associated with the Fe(tpa)/H_2O_2 combination in CH_3CN, from which a $[Fe^{V}(O)OH(tpa)]$ oxidant is proposed to form during catalysis.[13,14]

Table 3 compares the catalytic activity of the Fe(tpa)/H_2O_2 combination in CH_3CN and acetone with cyclohexane, *cis*-1,2-dimethylcyclohexane, and cyclooctene as probe substrates, together with corresponding Fe(tpa)/*t*BuOOH results in CH_3CN. It is clear that the conversion efficiency of H_2O_2 into products in acetone is about half of that in CH_3CN. This lower catalytic efficiency can be attributed to the formation of $[Fe^{III}_2O(O_2CCH_3)(tpa)_2]^{3+}$ as a byproduct in the acetone reaction, as observed at low temperature (Figure 5). The formation of the catalytically inactive $[Fe^{III}_2O(O_2CCH_3)(tpa)_2]^{3+}$ is clearly evidenced by the appearance of its characteristic visible spectrum[22] at the end of the catalytic run.

Interestingly, the product distribution observed for the Fe(tpa)/H_2O_2 combination in acetone is quite similar to that in CH_3CN and distinct from that by the Fe(tpa)/*t*BuOOH combination in CH_3CN. Both the alkane and alkene oxidation products observed for Fe(tpa)/H_2O_2 in acetone strongly suggest the dominant participation of a metal-based oxidant, as in the case of the Fe(tpa)/H_2O_2 combination, rather than that of an alkoxy radical that derives from O–O bond homolysis, as in the case of the Fe(tpa)/*t*BuOOH combination.[25,26]

As shown in Table 3, the hydroxylation of cyclohexane in acetone afforded an alcohol/ketone (A/K) ratio of 3.5, and the hydroxylation of the tertiary C–H group on *cis*-1,2-dimethylcyclohexane occurred with 93% retention of configuration, values approaching those of Fe(tpa)/H_2O_2 in CH_3CN. In contrast, the corresponding reactions with the Fe(tpa)/*t*BuOOH combination resulted respectively in an A/K ratio close to 1 and significant loss of configuration of the tertiary alcohol product, consistent with the formation of a long-lived alkyl radical. This long-lived radical is trapped by O_2 to afford the radical chain autoxidation products observed in air. Thus as in CH_3CN, alkane hydroxylation by Fe(tpa)/H_2O_2 in acetone still appears to be carried out by a high-valent metal–oxo oxidant that generates a short-lived alkyl radical, which is quickly trapped in a rebound step. Similar observations have been made by Feringa and co-workers in their comparison of the catalytic behavior of the isomeric Fe(N3Py-Me) complex in the two solvents with respect to alkane hydroxylation.[10]

The cyclooctene oxidation results in acetone also argue against the involvement of free alkoxyl radicals in the oxidation mechanism. The Fe(tpa)/H_2O_2 combination in acetone gave rise to cyclooctene oxide and *cis*-cyclooctane-1,2-diol as the major products in a ~1:1 ratio, just as in CH_3CN.

Table 3. Comparison of the reactivity of Fe^{II}(tpa)/ROOH combinations in CH_3CN and acetone.[a]

	Fe(tpa)/H_2O_2 CH_3CN[b]	Fe(tpa)/H_2O_2 acetone	Fe(tpa)/*t*BuOOH CH_3CN[c]
cyclohexane			
alcohol (A) TON	2.7	1.4	1.9 (4.0)[d]
ketone (K) TON	0.5	0.4	2.2 (n.d.)[d]
A/K	5	3.5	0.8[d]
cis-1,2-dimethylcyclohexane			
3°-ol TON[e]	3.8	0.9	1.6 (1.9)
% RC	>99%	93%	25% (39%)
cyclooctene			
epoxide TON	3.4	1.8	4.6 (0.4)[f]
% RC	>99%	>92%	98% (>90%)
cis-1,2-diol TON	4.0	1.7[g]	n.d.
% RC	>99%	63%	
epoxide/diol	1:1.2	1.1:1	
cyclooct-2-en-1-ol TON	n.d.	n.d.	n.d.(4.1)

[a] Catalytic oxidations are generally carried out by the introduction of 10 or 20 equivalents oxidant by syringe pump over 21–25 min to a solution of 0.7 mM catalyst in CH_3CN or acetone. Results are reported as the number of turnovers (TON) per 10 equivalents oxidant for comparison purposes. n.d. = not detected. [b] Results from references [13] and [14]. [c] Values in parentheses obtained from experiments under argon. [d] Results from reference [25] [e] Secondary alcohols and ketones observed but not quantified. [f] Several other minor oxidation products were detected. [g] Diols obtained exclusively as the acetonides.

While epoxidation was highly stereoselective (>92% RC), there is some loss of stereoselectivity in *cis*-dihydroxylation (63% RC). In contrast, cyclooctene oxidation by Fe(tpa)/*t*BuOOH in CH_3CN gave 4.6 equivalents of epoxide and a mixture of other minor oxidation products, indicated by the many small peaks observed in the GC trace. Under argon, the epoxide yield decreased significantly, and the principal product observed was the allylic alcohol. The absence of *cis*-diol product and the appearance of the allylic hydroxylation product reflect the involvement of a distinct oxidant for the Fe(tpa)/*t*BuOOH combination that gives rise mainly to the cyclooctenyl radical. (Interestingly, in the case of the Fe(N3Py-Me) species, cyclooctene oxidation in acetone afforded the expected *cis*-epoxide and the unexpected *trans*-diol![10] This surprising switch in stereoselectivity in dihydroxylation has not been rationalized and deserves further examination.).

The observation that the Fe(tpa)/H_2O_2 combination affords similar oxidation products in acetonitrile and acetone at room temperature yet exhibits different peroxo intermediates at low temperature suggests that the observed low-temperature intermediates may not relate to the room-temperature oxidation chemistry. This point has also been raised by Talsi and co-workers in their unsuccessful efforts to observe a substrate concentration dependence on the kinetics of decay of the $[Fe^{III}(tpa)(OOH)]^{2+}$ intermediate at low temperature.[16] However a rate-determining O–O bond cleavage step could mask the dependence on substrate concentration.

Scheme 2 compares the proposed intermediates derived from O–O bond cleavage for the three Fe(tpa) cases. As with the Fe^{III}(tpa)–OO*t*Bu intermediate, O–O bond homolysis of the Fe^{III}(tpa)–$OOC(CH_3)_2OH$ intermediate should produce the Fe^{IV}=O species and an alkoxyl radical. But unlike the readily diffusible *tert*-butoxyl radical, the alkoxyl radical derived from HHPP has a hydroxo group that could allow this alkoxyl species to remain coordinated to the iron center during catalysis (intermediate **B** in Scheme 2). Intermediate **B** could then effectively be considered as formally Fe^{V}, equivalent to intermediate **A**. The bound alkoxyl radical in **B** could act to abstract a hydrogen atom from cyclohexane to generate an alkyl radical that then readily combines with the nearby iron(IV)–oxo unit to form the alcohol product with little loss of stereochemistry. Alternatively, **B** may lose acetone and convert to intermediate **A** during room temperature catalysis. At low temperature, the alkoxyl radical could decompose by loss of methyl radical to yield the acetate that eventually bridges the (μ-oxo)diiron(III) unit obtained in the decay of the oxoiron(IV) species. The possibility for coordinating the 2-hydroxy-2-propoxyl radical highlights the importance of the available sixth site on the Fe(tpa) center. When this site is not available as in the case of the closely related Fe(N4Py)/H_2O_2 system,[27] the observed products resemble those derived from Fe(tpa)/*t*BuOOH and are attributed to the action of HO· and $[Fe^{IV}(O)(N4Py)]^{2+}$ formed by homolysis of $[Fe^{III}(N4Py)(OOH)]^{2+}$.

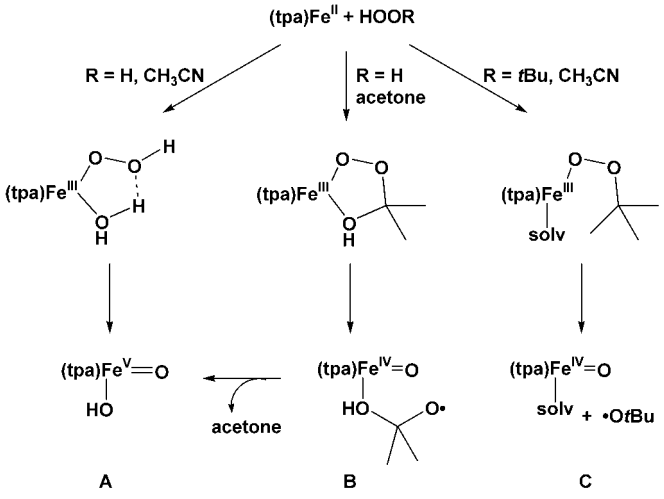

Scheme 2.

Conclusions

The $[Fe^{III}(tpa)(OOH)]^{2+}$ intermediate in CH_3CN is only the second iron(III) hydroperoxide complex to be fully verified by resonance Raman isotope-labeling experiments to have an end-on hydroperoxide ligand and corroborates the results reported for $[Fe^{III}(N4Py)(\eta^1\text{-}OOH)]^{2+}$.[15] Together these two complexes establish the Raman spectroscopic signature for this growing class of complexes relevant to oxygen activation mechanisms of iron enzymes.[2,3]

However, unlike $[Fe^{III}(N4Py)(\eta^1\text{-}OOH)]^{2+}$, which is formed from the reaction of an Fe^{II}(N4Py) complex and H_2O_2 in either CH_3CN or acetone, a distinct species is obtained for the reaction of the Fe^{II}(tpa)-type complex and H_2O_2 in acetone that is stable only at −90°C. Spectroscopic evidence is presented for the first example of an Fe^{III}–{κ^2-$OOC(CH_3)_2OH$}-type complex. The different outcome is proposed to arise mainly from the availability of a coordination site on the tetradentate tpa complex that stabilizes the proposed peroxoacetone adduct through the formation of a five-membered chelate ring. These findings serve as a cautionary note for interpreting data for H_2O_2 intermediates generated in acetone as a solvent.

At −50°C, the peroxoacetone intermediate converts to an Fe^{IV}=O species, resembling the species obtained from the stoichiometric reaction of Fe^{II}(tpa) and peracids and from the decay of the corresponding Fe^{III}–OO*t*Bu intermediate. Like the latter, the Fe^{IV}=O species is formed through the homolytic cleavage of the $[Fe^{III}(tpa)\{\kappa^2\text{-}OOC(CH_3)_2OH\}]^{2+}$ intermediate, which is accelerated by pyridine *N*-oxide. Indeed the enthalpy of activation obtained for either the decay of $[Fe^{III}(tpa)\{\kappa^2\text{-}OOC(CH_3)_2OH\}]^{2+}$ or the formation of $[Fe^{IV}(O)(tpa)]^{2+}$, $\Delta H^{\ddagger} = 54(3)$ kJ mol^{-1}, agrees well with that previously determined for $[Fe^{III}(tpa)(OOtBu)]^{2+}$ decay in CH_3CN.[24] Thus this once elusive species turns out to be easily prepared under the appropriate conditions.

The observed decay of $[Fe^{III}(tpa)\{\kappa^2\text{-}OOC(CH_3)_2OH\}]^{2+}$ by O–O bond homolysis at low temperature to form $[Fe^{IV}(O)(tpa)]^{2+}$ and, presumably, the 2-hydroxy-2-propoxyl radical initially suggests that oxidation catalysis by Fe^{II}(tpa)/

H_2O_2 in acetone should resemble Fe^{II}(tpa)/*t*BuOOH in giving products derived mainly from alkoxyl-radical-initiated reactions. Instead the products resemble those of Fe^{II}(tpa)/H_2O_2 in CH_3CN, and high stereoselectivity is observed for the products of *cis*-1,2-dimethylcyclohexane hydroxylation and cyclooctene *cis*-dihydroxylation. These results suggest that the $[Fe^{IV}(O)(tpa)]^{2+}$/alkoxyl radical combination (intermediate **B** in Scheme 2) behaves effectively like the $[Fe^{V}(O)(OH)(tpa)]^{2+}$ species (intermediate **A** in Scheme 2), which is proposed to be the oxidant in Fe^{II}(tpa)/H_2O_2 oxidation catalysis in CH_3CN. The contrast in catalytic behavior between Fe^{II}(tpa)/H_2O_2 and Fe^{II}(N4Py)/H_2O_2 in either acetonitrile or acetone serves to emphasize how important the available sixth site is for catalysis. Our observations in acetone thus reveal subtleties and complexities of the Fe^{II}(tpa)/H_2O_2 reaction landscape that merits further exploration.

Experimental Section

Materials and synthesis: All reagents were purchased from commercial sources and used as received, unless noted otherwise. CH_3CN and CH_2Cl_2 were distilled from CaH_2 and acetone from $MgSO_4$.

Syntheses of $[Fe^{II}(tpa)(OTf)_2]$ and $[Fe^{II}(5\text{-}Me_3\text{-}tpa)(OTf)_2]$: The complexes were synthesized under argon by overnight stirring of equimolar amounts of $[Fe^{II}(OTf)_2]\cdot 2\,CH_3CN$[28] and tpa or 5-$Me_3$-tpa[29] in CH_2Cl_2, as previously described for the tpa complex.[23] Big greenish yellow crystals were obtained by room temperature vapor diffusion of diethyl ether into the solutions (ca. 70–80% yield). Elemental analysis calcd (%) for $[Fe^{II}(5\text{-}Me_3\text{-}tpa)(OTf)_2]$, $C_{23}H_{24}F_6FeN_4O_6S_2$: C 40.24, H 3.52, N 8.16, S 9.34, F 16.61; found: C 40.31, H 3.70, N 8.18, S 9.40, F 16.51.

Generation of $[Fe^{III}(tpa)(\eta^1\text{-}OOH)]^{2+}$: Treatment of $[Fe^{II}(tpa)(OTf)_2]$ in CD_3CN, CH_3CN/CD_2Cl_2 (1:1), or CD_3CN/THF (4:1) at −40 °C or lower with 10 equiv H_2O_2 (typically 2% by volume in dry solvent) resulted in the formation of $[Fe^{III}(tpa)(OOH)]^{2+}$, which was then fully characterized by resonance Raman spectroscopy.

Generation of $[Fe^{III}(tpa)(\kappa^2\text{-}OOC(CH_3)_2OH)]^{2+}$: Treatment of $[Fe^{II}(tpa)(OTf)_2]$ in acetone at −90 °C with 1.5–3 equiv H_2O_2 (typically 2% by volume in dry solvent) resulted in the formation of $[Fe^{III}(tpa)\{OOC(CH_3)_2OH\}]^{2+}$, which was characterized by UV/Vis, EPR, and resonance Raman spectroscopy.

Physical methods: Electronic absorption spectra were recorded on a Hewlett–Packard 8453 diode array spectrophotometer (190–1100 nm scan range) in quartz cuvettes cooled to the desired temperature with an Unisoku USP-203 cryostat. Resonance Raman spectra were collected on an Acton AM-506 spectrometer (2400-groove grating) by using Kaiser Optical holographic super-notch filters with a Princeton Instruments liquid N_2-cooled (LN-1100PB) CCD detector with 4 cm^{-1} or 2 cm^{-1} spectral resolution. Spectra were obtained by a back-scattering geometry on liquid N_2 frozen samples using 514.5 nm laser excitation from a Spectra Physics 2030–15 argon ion laser or 568.2 nm using the same argon laser in combination with a 375B CW dye (Rhodamine 6G). Raman frequencies were referenced to indene. EPR spectra were recorded on a Bruker EPP 300 spectrometer equipped with an Oxford ESR 910 liquid helium cryostat and an Oxford temperature controller. Electrospray mass spectra were taken using a Bruker BioTOF II instrument.

Oxidation catalysis experiments: A solution of either H_2O_2 or *t*BuOOH (70 mM, 0.30 mL, 10 equiv/Fe) was added at the rate of 14 μL min^{-1} via syringe pump to a stirred solution of a substrate (1.05 mmol) and $[Fe^{II}(tpa)(OTf)_2]$ (2.1 μmol Fe) in solvent (2.6 mL) at room temperature. For anaerobic experiments, reactions were performed under argon after degassing all solutions. The dilute H_2O_2 solutions in CH_3CN or acetone were prepared from 35 wt% aqueous H_2O_2. The H_2O_2/acetone solution was dried over $MgSO_4$ and filtered before use in order to control the water content. The concentration of the peroxide was not affected by this drying process, as confirmed by iodometric titration. The dilute *t*BuOOH solution in CH_3CN was prepared from 70 wt% aqueous *t*BuOOH. Each organic substrate (cyclohexane, *cis*-1,2-dimethylcyclohexane, or cyclooctene) was passed through a short column of basic alumina-I before use. The reaction solutions were stirred for an additional 5 min after syringe pumping was complete. For the alkane oxidation reactions, the solutions were then passed through a short silica column to remove the catalyst. The column was then washed with 3–4 mL of ethyl acetate. Internal standard (naphthalene, 13.7 mM in CH_3CN, 0.50 mL) was added before GC analysis. At the end of the cyclooctene oxidation reactions, the solutions were treated with acetic anhydride (0.5–1.0 mL) and 1-methylimidazole (0.1 mL) to acetylate the diol products for facile analysis, and an internal standard (naphthalene, 13.7 mM in CH_3CN, 0.50 mL) was added. After 15 min of stirring, chloroform and ice were added to the reaction solution. The organic layer was then washed consecutively with 1N H_2SO_4, sat. $NaHCO_3$, and water, dried over $MgSO_4$, and subjected to GC analysis.

Acknowledgments

This work was supported by the National Institutes of Health (GM-33162), the Petroleum Research Fund of the American Chemical Society (38602-AC), and the US Department of Energy (DE-FG02-03ER15455).

[1] E. I. Solomon, T. C. Brunold, M. I. Davis, J. N. Kemsley, S.-K. Lee, N. Lehnert, F. Neese, A. J. Skulan, Y.-S. Yang, J. Zhou, *Chem. Rev.* **2000**, *100*, 235.
[2] J.-J. Girerd, F. Banse, A. J. Simaan, *Struct. Bonding* **2000**, *97*, 143.
[3] M. Costas, M. P. Mehn, M. P. Jensen, L. Que, Jr., *Chem. Rev.* **2004**, *104*, 939.
[4] E. D. Coulter, J. P. Emerson, D. M. Kurtz, Jr., D. E. Cabelli, *J. Am. Chem. Soc.* **2000**, *122*, 11555.
[5] C. Mathé, T. A. Mattioli, O. Horner, M. Lombard, J.-M. Latour, M. Fontecave, V. Nivière, *J. Am. Chem. Soc.* **2002**, *124*, 4966.
[6] A. Karlsson, J. V. Parales, R. E. Parales, D. T. Gibson, H. Eklund, S. Ramaswamy, *Science* **2003**, *299*, 1039.
[7] E. Skrzypczak-Jankun, R. A. Bross, R. T. Carroll, W. R. Dunham, M. O. Funk, Jr., *J. Am. Chem. Soc.* **2001**, *123*, 10814.
[8] R. M. Burger, *Struct. Bonding* **2000**, *97*, 287.
[9] K. Chen, M. Costas, L. Que, Jr., *J. Chem. Soc. Dalton Trans.* **2002**, 672.
[10] M. Klopstra, G. Roelfes, R. Hage, R. M. Kellogg, B. L. Feringa, *Eur. J. Inorg. Chem.* **2004**, 846.
[11] C. Kim, K. Chen, J. Kim, L. Que, Jr., *J. Am. Chem. Soc.* **1997**, *119*, 5964.
[12] R. Y. N. Ho, G. Roelfes, B. L. Feringa, L. Que, Jr., *J. Am. Chem. Soc.* **1999**, *121*, 264.
[13] K. Chen, L. Que, Jr., *J. Am. Chem. Soc.* **2001**, *123*, 6327.
[14] K. Chen, M. Costas, J. Kim, A. K. Tipton, L. Que, Jr., *J. Am. Chem. Soc.* **2002**, *124*, 3026.
[15] G. Roelfes, V. Vrajmisu, K. Chen, R. Y. N. Ho, J.-U. Rohde, C. Zondervan, R. M. la Crois, E. P. Schudde, M. Lutz, A. L. Spek, R. Hage, B. L. Feringa, E. Münck, L. Que, Jr., *Inorg. Chem.* **2003**, *42*, 2639.
[16] M. V. Lobanova, K. P. Bryllakov, E. A. Duhan, E. P. Talsi, *Mendeleev Commun.* **2003**, 175.
[17] Y. Zang, J. Kim, Y. Dong, E. C. Wilkinson, E. H. Appelman, L. Que, Jr., *J. Am. Chem. Soc.* **1997**, *119*, 4197.
[18] J. Kim, E. Larka, E. C. Wilkinson, L. Que, Jr., *Angew. Chem.* **1995**, *107*, 2191; *Angew. Chem. Int. Ed. Engl.* **1995**, *34*, 2048.
[19] N. Lehnert, R. Y. N. Ho, L. Que, Jr., E. I. Solomon, *J. Am. Chem. Soc.* **2001**, *123*, 8271.
[20] M. C. V. Sauer, J. Edwards, *J. Phys. Chem.* **1971**, *75*, 3004.
[21] M. Lubben, A. Meetsma, E. C. Wilkinson, B. Feringa, L. Que, Jr., *Angew. Chem.* **1995**, *107*, 1610; *Angew. Chem. Int. Ed. Engl.* **1995**, *34*, 1512.
[22] R. E. Norman, S. Yan, L. Que, Jr., J. Sanders-Loehr, G. Backes, J. Ling, J. H. Zhang, C. J. O'Connor, *J. Am. Chem. Soc.* **1990**, *112*, 1554.

[23] M. H. Lim, J.-U. Rohde, A. Stubna, M. R. Bukowski, M. Costas, R. Y. N. Ho, E. Münck, W. Nam, L. Que, Jr., *Proc. Natl. Acad. Sci. USA* **2003**, *100*, 3665.
[24] J. Kaizer, M. Costas, L. Que, Jr., *Angew. Chem.* **2003**, *115*, 3799; *Angew. Chem. Int. Ed.* **2003**, *42*, 3671.
[25] J. Kim, R. G. Harrison, C. Kim, L. Que, Jr., *J. Am. Chem. Soc.* **1996**, *118*, 4373.
[26] P. A. MacFaul, K. U. Ingold, D. D. M. Wayner, L. Que, Jr., *J. Am. Chem. Soc.* **1997**, *119*, 10594.
[27] G. Roelfes, M. Lubben, R. Hage, L. Que, Jr., B. L. Feringa, *Chem. Eur. J.* **2000**, *6*, 2152.
[28] A. Diebold, K. S. Hagen, *Inorg. Chem.* **1998**, *37*, 215.
[29] Y. Dong, H. Fujii, M. P. Hendrich, R. A. Leising, G. Pan, C. R. Randall, E. C. Wilkinson, Y. Zang, L. Que, Jr., B. G. Fox, K. Kauffmann, E. Münck, *J. Am. Chem. Soc.* **1995**, *117*, 2778.

Received: May 14, 2004
Published online: September 2, 2004

